Proceedings of the 21st ICSMGE, Vienna, Austria, 14 – 19 June 2026. Pistrol, Adam & Schweiger (eds.)
Published by: ÖGG, Austrian Society for Geomechanics, Salzburg, Austria, ISBN 978-3-9503898-4-5
https://doi.org/10.53243/ICSMGE2026-339

Quantifying the Influence of Preferential Flow on Soil Infiltration in the Loess Plateau

Yukai Fu, Dantong Lin
Key Laboratory of Western China's Environmental Systems (Ministry of Education), College of Earth and Environmental Sciences, Lanzhou University, Lanzhou, Gansu, China

ABSTRACT: Since 1999, China has implemented large-scale vegetation restoration on the Loess Plateau. The continuous development of plant root systems in the loess has induced changes in surface soil structure, while root-induced macropores have significantly enhanced the occurrence of preferential flow. However, studies on profile-scale saturated hydraulic conductivity and water infiltration under such conditions remain limited. This study employs high-resolution remote sensing datasets, including Leaf Area Index (LAI) and soil texture information, to quantify how vegetation-induced soil structural changes influence the hydraulic properties of the Loess Plateau based on 2017 observations. The results indicate that macropores increase the regional average saturated hydraulic conductivity by approximately 29.8%. Using CMIP6 projections for 2075, the Philip infiltration model was applied to compare soil water infiltration between the two rainy seasons. The findings show that in 2017, preferential flow contributed an additional 2% – 40% infiltration relative to matrix flow alone, whereas by 2075, the proportion of infiltration enhanced by preferential flow is projected to increase substantially, potentially reaching 5% – 80%. Furthermore, both vegetation conditions and rainfall intensity are positively correlated with the magnitude of infiltration enhancement caused by preferential flow. These findings emphasize the importance of considering soil structural changes during vegetation restoration, providing valuable insights for ecological restoration and water resource management in the Loess Plateau region.

KEYWORDS: Vegetation restoration, soil structure, preferential flow, saturated hydraulic conductivity, Philip infiltration model.

1 INTRODUCTION

The Loess Plateau is internationally recognized as an extremely fragile ecological environment. Due to the influence of climatic conditions and long-term anthropogenic damage, the local ecological function has been impaired and the environment has deteriorated (Wen and Deng, 2020; Wang et al., 2023a). In order to improve the fragile ecological environment, the Loess Plateau region of China has implemented numerous long-term forest vegetation restoration projects. Extensive sloping farmlands have been converted into grasslands and woodlands, resulting in a significant improvement in vegetation cover (Zhang et al., 2021; Guan et al., 2024). Vegetation primarily mitigates shallow landslides through root reinforcement and the promotion of soil structure development (Lehmann, Von Ruette and Or, 2019). This enhanced soil structure improves the infiltration and drainage capacity of hillslopes, thereby delaying the onset of landslide triggering and effectively reducing the occurrence of rainfall-induced landslides (Fan et al., 2022).

Several studies have demonstrated that vegetation restoration increases both the extent and depth of soil infiltration, significantly enhancing the soil's infiltration capacity and intensifying the occurrence of preferential flow (PF) during the infiltration process (Ren et al., 2016; Guan et al., 2024). Preferential flow refers to the rapid infiltration of water through macropores in the soil, bypassing the soil matrix. It is often induced by factors such as plant root systems, soil fauna activity, or desiccation cracks (Guo et al., 2018). Preferential flow has a faster migration speed and is an important process affecting hydrological, geochemical and ecological cycles. Research on preferential flow has predominantly focused on point-scale experiments, such as dye tracing and profile observations (Wang et al., 2020a). While these methods have revealed the mechanisms underlying preferential flow, our understanding of its spatial distribution characteristics and influencing factors at the regional scale remains limited (Kang et al., 2023).

Soil saturated hydraulic conductivity is one of the most critical soil hydraulic parameters reflecting soil infiltrability (Zhu et al., 2020). Most soil hydraulic information used in Earth System Models is derived from pedotransfer functions, which estimate hydraulic parameters based on easily measurable soil properties. This parameterization heavily relies on soil texture, while largely neglecting the critical role of soil structure shaped by biophysical processes. Incorporating soil structure into models can significantly alter infiltration dynamics in vegetated regions (Fatichi et al., 2020). While saturated hydraulic conductivity has been widely studied, the majority of research has centered on land use effects, with limited efforts made to quantitatively evaluate the impact of revegetation on K_s profiles at a regional scale. Some studies have utilized long-term soil moisture monitoring networks across multiple sites to investigate the propagation of wetting fronts during rainfall events by defining infiltration events. These studies have examined the effects of different vegetation types and soil properties on infiltration metrics, which enhances our understanding of the mechanisms of preferential flow and the hydrological cycle at small scales (Kang et al., 2022; Xue et al., 2024). However, when extended to larger regions, such analyses are often limited by the lack of observed data.

To address this issue, we applied a pedotransfer function (PTF) adapted to the Loess Plateau to estimate regional saturated hydraulic conductivity. Moreover, based on the revegetation status and soil physicochemical properties in the Loess Plateau, we corrected the regional saturated hydraulic conductivity using leaf area index and soil sand content data, in order to account for the influence of soil structure on saturated permeability. Based on this parameterization scheme, the Philip infiltration model was employed to analyze spatial variations in water infiltration resulting from vegetation restoration across the Loess Plateau. Quantitative evaluations of preferential infiltration are helpful in calculating slope seepage, evaluating slope stability, and researching landslide initiation mechanisms (Ma et al., 2022).

2 MATERIALS AND METHODS

2.1 *Study area*

This study was conducted on the Loess Plateau of China (33°43′–41°16′N, 100°54′–114°33′E), which covers an area of approximately 640,000 km² and contains the world's thickest loess deposits. The region is characterized by a temperate continental monsoon climate, with mean annual precipitation

increasing from northwest to southeast, ranging from 150 mm to 820 mm, and mostly concentrated between June and September. The mean annual temperature ranges from 3.6°C to 14.3°C, with an average elevation between 1000 and 1500 meters, as presented in Figure 1a.

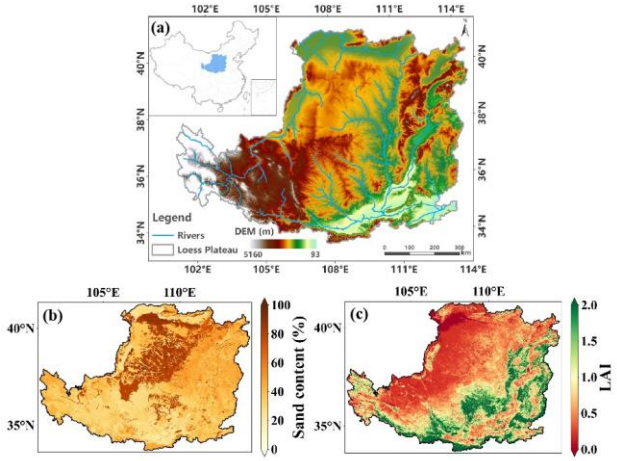

Figure 1. Location of the Loess Plateau and the Spatial Distribution of Soil Texture and LAI.

Figure 1b and 1c illustrate the spatial distribution of soil texture and LAI, respectively. The soil texture exhibits a clear gradient from northwest to southeast, transitioning progressively from sandy soils to light loam, medium loam, and finally heavy loam. In Figure 1b, the sand content decreases from approximately 50% in the northwest to about 5% in the southeast (Chen, Shao and Li, 2008; Fu et al., 2017). Among various soil properties, sand content has a significant influence on saturated hydraulic conductivity, as soils with higher sand content generally exhibit greater water conductivity (Kang et al., 2021). Correspondingly, vegetation types change across the plateau from desert and desert steppe in the northwest to typical steppe and forest steppe in the southeast, as shown in Figure 1c, LAI also exhibits a spatial distribution pattern of being lower in the northwest and higher in the southeast.

Table 1. Description of data sources

Data sources	Variable name	Time resolution	Space resolution
CMFD	Rainfall intensity	3 h	0.1°
China Soil	Sand, clay, bulk density, porosity	-	~1 km
MODIS	LAI	8 d	500 m
SMCI	Soil water content	1 d	~1 km
CMIP6	LAI, precipitation,	1 d	~1°

2.2 *Data and processing*

Table 1 summarizes the data sources used in this study, including their respective spatial and temporal resolutions. The precipitation data used in this study are derived from the China Meteorological Forcing Dataset (CMFD) (Yang et al., 2010; He et al., 2020), which includes meteorological variables such as precipitation and near-surface air temperature. It is generated by integrating observations from 740 national meteorological stations across China, and its accuracy and reliability have been verified in multiple studies (Chen et al., 2011; Yang et al., 2017). Soil texture data are obtained from a China soil dataset developed for land surface modeling (Shangguan et al., 2013), which is based on 8,595 soil profiles collected during the second national soil survey. The dataset includes soil properties such as profile depth, sand, silt, clay contents, bulk density, and porosity. The LAI used in this study is obtained from the Moderate Resolution Imaging Spectroradiometer (MODIS) product (Myneni, Knyazikhin and Park, 2015). Soil moisture data are taken from the SMCI1.0 (Soil Moisture of China by in situ data, version 1.0) dataset, which provides high-quality 1 km soil moisture data across China (Li et al., 2022). The LAI data were obtained from the CMIP6 SSP245 scenario using the CMCC-ESM2 model, which has a native spatial resolution of approximately 0.9° × 1.25°. Precipitation data were derived from the CMIP6 SSP245 outputs of the BCC-CSM2-MR model, with a spatial resolution of roughly 1.1° × 1.1°. All datasets were downloaded from the Earth System Grid Federation (ESGF) data portal (https://esgf-node.llnl.gov/search/cmip6/). Data processing and calculation were performed using ArcGIS and Python. To meet spatial resolution requirements, bilinear interpolation was applied to the LAI, SMCI, and soil texture datasets, and the time series of each dataset was temporally aligned.

2.3 *Estimation of soil saturated hydraulic conductivity*

Over the years, the growth and development of vegetation roots on the Loess Plateau have gradually altered the structure of surface soils. To account for the impact of vegetation restoration on macropores in the soil, previous study has proposed using LAI as an indicator of soil structural changes (Fatichi et al., 2020). Equation (1) was employed to establish the relationship between the saturated hydraulic conductivity of textural soil and that of structured soil (Bonetti, Wei and Or, 2021):

$$K_{\mathrm{s}} = K_{\mathrm{s,max}} - \frac{K_{\mathrm{s,max}} - K_0}{1 + \left(\frac{LAI}{\alpha}\right)^{\beta}} \quad (1)$$

Based on this parameterization scheme, high LAI corresponds to fully developed soil structure (higher saturated hydraulic conductivity), while low LAI indicates undeveloped structure. Among them, the shape parameters α and β were assigned values of 4.5 and 5, respectively, based on the calibration by (Bonetti, Wei and Or, 2021) of the relationship between soil saturated hydraulic conductivity and LAI in a forest in Nicaragua. In this context, K_0 represents the saturated hydraulic conductivity related only to soil texture, K_s represents the saturated hydraulic conductivity under structured soil conditions, this is attributed to vegetation restoration (Pan et al., 2023), and $K_{s,max}$ is the maximum saturated hydraulic conductivity when plant roots are fully developed within soil pores. As shown in Table 1, using LAI data and soil texture information from June 2017 on the Loess Plateau, during this period, we calculated both K_0 and K_s across the Loess Plateau region.

The PFTs are employed to determine the value of K_0 on the Loess Plateau. The implementation of this method relies on a large number of field experiments, based on measured data, developed regionally applicable PTFs (as shown in Equation (2)) using clay content, sand content, and bulk density (BD), which are particularly suitable for soils in the Chinese Loess Plateau (Zhu, Zhang and Zhang, 2022):

$$K_{\mathrm{S}} = 0.365 + 0.015 f_{\mathrm{clay}} + 0.031 f_{\mathrm{sand}} - 0.748 f_{\mathrm{bd}} \quad (2)$$

where f_{clay} and f_{sand} represent the fractions of clay and sand in the soil, respectively, and f_{bd} denotes the bulk density.

Both $K_{\text{s,max}}$ and K_{s} are affected by the sand content in the soil. Existing studies have shown that soil structure has a more pronounced effect on finer-textured soils (Singh et al., 2018; Parewa et al., 2023), as shown in Equation (3):

$$\log\frac{K_{\text{s,max}}}{K_0} = 3.5 - 1.5 \bullet {f_{\text{sand}}}^m \tag{3}$$

where m is the soil shape parameter.

2.4 *Philip infiltration*

To investigate the impact of vegetation restoration on soil saturated hydraulic conductivity, we used the two-term Philip model to simulate the infiltration process. According to this model, the infiltration rate is given by:

$$i(t) = \frac{S}{2}t^{-\frac{1}{2}} + A \tag{4}$$

where t is time, S is the soil sorptivity, which depends on soil properties, porosity, and initial soil moisture conditions. The steady-state infiltration rate, A, is set as one-third of the saturated hydraulic conductivity. In this study, two cases are considered: (1) using K_0 (texture-dependent saturated conductivity) and (2) using K_s (structure-influenced saturated conductivity), allowing comparison between texture-dominated and structured soil conditions. The first term in the equation describes the influence of capillary forces, while the second term represents the contribution of gravity.

$$t_{\text{e}} = \frac{S^2}{4(r-A)^2} \tag{5}$$

$$t_{\text{p}} = \frac{S^2\left(r - \frac{A}{2}\right)}{2r(r-A)^2} \quad (if\ \ r > A) \tag{6}$$

$$t_{\text{p}} = \infty \quad (if\ \ r \le A) \tag{7}$$

where the effective ponding time t_e refers to the time when the infiltration rate i equals the rainfall rate r. The actual ponding time t_p is determined by equating the cumulative infiltration.

$$i = r \quad (if\ \ t \le t_p) \tag{8}$$

$$i = \frac{S}{2}\left(t - t_{\text{p}} + t_{\text{e}}\right)^{-\frac{1}{2}} + A \quad (if\ \ t > t_{\text{p}}) \tag{9}$$

Soil moisture characteristic may be modeled as a power curve combined with a short parabolic section near saturation to represent gradual air entry, as shown in Equation (10) (Clapp and Hornberger, 1978).

$$\psi = \bar{\psi}(W)^{-b} \tag{10}$$

$$W = \frac{\theta}{\theta_{\text{s}}} \tag{11}$$

where θ_s is the total porosity of the soil. Both $\bar{\psi}$, the air-entry suction point, and the exponent b are empirical and must be estimated.

$$k = (W)^{2b+3} \tag{12}$$

where k is the relative hydraulic conductivity.

$$S = [2K_{\text{s}}\psi_{\text{f}}\theta_{\text{s}}(1 - W_{\text{tc}})]^{\frac{1}{2}} \tag{13}$$

A first approximation for sorptivity is derived by equating the Green-Ampt equation (considering a surface pressure of zero) to Philip's two-term infiltration equation.

$$\psi_{\text{f}} = \left[\frac{(2b+3)}{(b+3)}\right]\psi_{\text{s}} \tag{14}$$

A comparison with the exact solution of the unsaturated flow equation reveals only minor discrepancies, indicating that this result is sufficiently accurate for a wide range of applications. The soil sorptivity S can be obtained analytically as (Fatichi et al., n.d.):

$$S = \left[\frac{-2bK_0\bar{\psi}(\phi - \theta_0)}{(3+b)\phi^{b+3}}\left(\phi^{b+3} - \theta_0^{b+3}\right)\right]^{\frac{1}{2}} \tag{15}$$

where S is calculated under the assumption that soil structure does not affect soil sorptivity, using the unstructured saturated hydraulic conductivity K_0. The influence of soil structure is incorporated by modifying the gravitational term A.

2.5 *Brooks-Corey parameters*

The Brooks-Corey model (Brooks and Corey, 1964) established a power-law relationship between soil volumetric water content θ and capillary pressure head h, expressed as:

$$\frac{\theta - \theta_{\text{r}}}{\phi - \theta_{\text{r}}} = \begin{cases} \left(\frac{h_{\text{b}}}{h}\right)^{\lambda}, & h > h_{\text{b}} \\ 1, & h \le h_{\text{b}} \end{cases} \tag{16}$$

where ϕ is the soil porosity, $\text{cm}^3\ \text{cm}^{-3}$, θ_r is the residual water content, $\text{cm}^3\ \text{cm}^{-3}$; h_b is air-entry pressure, cm; and λ is pore size distribution index.

The Brooks-Corey parameters can be estimated by using sand and clay content along with soil bulk density (Campbell and Shiozawa, 1992). By setting the residual water content in Equation (16) to zero, the Brooks-Corey model can be simplified to:

$$h = h_{\text{b}}\left(\frac{\theta}{\theta_{\text{s}}}\right)^{-b} \tag{17}$$

The parameters in Equation (17), estimated from two data sets for British soils, were found to be:

$$h_{\text{es}} = -0.05{d_{\text{s}}}^{-\frac{1}{2}} \tag{18}$$

$$b = -20h_{\text{es}} + 0.2\sigma_{\text{g}} \tag{19}$$

where the value of h_{es} corresponds to the air entry pressure at a standard bulk density, ρ_b of 1.3 g cm^{-3}. The proposed adjustment for bulk density is:

$$h_{\text{b}} = h_{\text{es}}\left(\frac{\rho_b}{1.3}\right)^{0.67b} \tag{20}$$

The geometric mean diameter d_s and geometric standard deviation σ_g are given by:

$$d_{\text{s}} = \exp\left(-0.80 - 0.0317f_{\text{silt}} - 0.0761f_{\text{clay}}\right) \tag{21}$$

$$\sigma_{\text{g}} = \exp\left(0.133f_{\text{silt}} + 0.477f_{\text{clay}} - \ln^2 d_{\text{s}}\right)^{\frac{1}{2}} \tag{22}$$

where f_{silt} represents the fraction of silt in the soil.

3 RESULTS AND DISCUSSIONS

3.1 *Soil Saturated Hydraulic Conductivity Distribution in the Loess Plateau*

To investigate the impact of vegetation restoration on soil saturated hydraulic conductivity, we compared the results of saturated hydraulic conductivity between textural soils and structured soils. As shown in Figure 2, due to the widespread

distribution of desert areas in the northwestern Loess Plateau, where vegetation is sparse and soil texture is predominantly sandy, the K_0 in this region is relatively high, mainly ranging from 80 to 120 mm/h. In contrast, the southern region has denser vegetation and finer soil texture, resulting in lower K_0 values ranging from 20 to 50 mm/h. In the northeastern part, K_0 generally falls between 50 and 80 mm/h. Due to variations in topography and landforms across the Loess Plateau, the textural soils are strongly influenced by sand content, leading to a highly heterogeneous spatial distribution of saturated hydraulic conductivity across the region.

As shown in Figure 3, due to the implementation of vegetation restoration on the Loess Plateau, we incorporated corrections to account for the influence of plant root systems on K_s. In areas with good vegetation cover in the southern region, K_s showed a significant increase compared to the K_0, rising from 60 – 80 mm/h to approximately 100 mm/h. These values are close to those obtained from field experiments by other researchers in the Loess Plateau (Pan et al., 2023). In contrast, in areas with poor vegetation restoration, K_s remained largely unchanged.

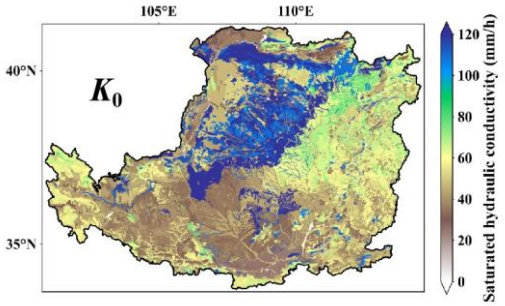

Figure 2. Saturated Hydraulic Conductivity of Textural Soils in the Loess Plateau

According to the PTFs calculations, the K_0 in the northwest is relatively high, while in the southeast it is lower. As shown in Figure 4, the average K_0 across the entire region is approximately 61.95 mm/h. After accounting for the influence of soil structures on soil properties, the K_s in the Loess Plateau increases to 80.47 mm/h, representing a 29.8% increase. The complex root systems of surface plants in this region contribute to the formation of soil structures in the soil, which significantly affect saturated hydraulic conductivity.

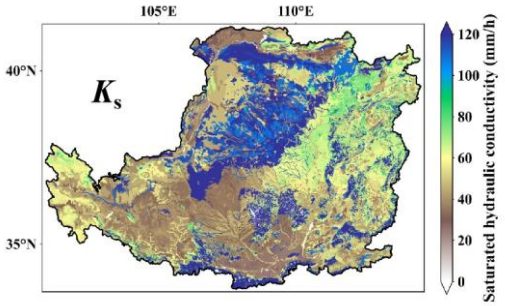

Figure 3. Saturated Hydraulic Conductivity of Structured Soils in the Loess Plateau

This spatial variability indicates that soil structures have a substantial impact on soil properties and regional hydrological processes. In the subsequent Philip infiltration analysis, we further investigate the infiltration behavior of surface soil moisture. Considering this influence is essential for improving the accuracy of regional hydrological modeling, water resource management, and planning.

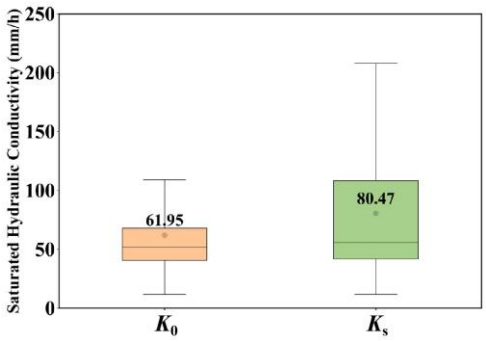

Figure 4. Boxplot of Saturated Hydraulic Conductivity with and Without Considering Soil Structure

3.2 *Quantifying hydrologic effects of soil structure*

Following the parameterization of saturated hydraulic conductivity across the Loess Plateau, the Philip infiltration model was applied to simulate infiltration for June 2017 and July 2075. In the Philip model, the relationship between rainfall rate and the gravity term A is particularly important. The value of the gravity term A depends on both the soil saturated hydraulic conductivity and its texture. When the rainfall rate is lower than the gravity term, the infiltration rate equals the rainfall rate. When the rainfall rate exceeds the gravity term, the infiltration rate i is controlled by the equivalent and actual ponding times. By integrating the infiltration rate over time, we obtained the daily cumulative infiltration for each grid cell for the two periods, with the temporal resolution determined by the soil moisture dataset and the CMIP6 forcing data.

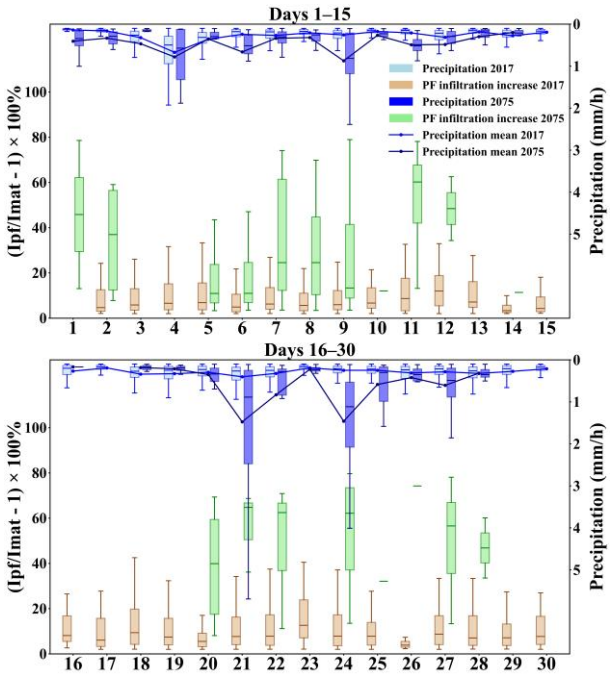

Figure 5. Boxplot of Rainy-Season Precipitation and Soil Infiltration Increase Ratio over the Loess Plateau for the Years 2017 and 2075

Due to the highly uneven spatial and temporal distribution of rainfall across the Loess Plateau, precipitation in most grid cells was negligible. To better capture the influence of soil macropore structure on infiltration, we analyzed cumulative infiltration only for grid cells where the rainfall rate exceeded 0.1 mm/h. This approach enabled a more comprehensive assessment of soil water infiltration under different rainfall intensities (light, moderate, heavy, and torrential rain), and facilitated statistical comparisons between total rainfall and the contributions of preferential flow.

As shown in Figure 5, the proportion of infiltration contributed by preferential flow is positively correlated with rainfall rate, with similar temporal trends. This is because, in most infiltration-effective grid cells (mainly experiencing light to moderate rain with a near-normal distribution), infiltration is primarily governed by rainfall rate. However, when rainfall rate increases, the contribution from macropore structure becomes significant, enhancing matrix flow-based infiltration by 2% – 80%. Previous studies conducted in the Loess Plateau using point-scale soil experiments have reported that preferential flow contributed approximately 11% – 88% to total infiltration (Xiang et al., 2019; Zhang et al., 2019; Wang et al., 2020b; 2023b; Zhao and Wang, 2021). These values are comparable to the range of preferential flow contributions estimated at the regional scale in this study. During the 2017 rainy season on the Loess Plateau, preferential flow contributed approximately 2% – 40% additional infiltration. With the increasing frequency of extreme weather events under global climate change, CMIP6 projections indicate that by the 2075 rainy season, intensified and highly variable rainfall—together with markedly improved vegetation conditions—will substantially enhance the role of preferential flow. The proportion of infiltration attributable to preferential flow is projected to rise to 5% – 80%, representing roughly a one- to threefold increase compared with 2017.

This demonstrates that preferential flow on the Loess Plateau is mainly induced by macropores formed by plant root systems during heavy rainfall events. Therefore, we conducted a statistical analysis of LAI and various rainfall intensities across the entire Loess Plateau for June 2017. As shown in Figure 6, under light rainfall, soil saturated hydraulic conductivity was much higher than the rainfall rate for most grid cells. Thus, in Philip model calculations, infiltration equaled rainfall, resulting in negligible increases (0.1% – 2%) due to preferential flow. With increasing rainfall intensity, some grid cells showed higher infiltration ratios, indicating that preferential flow frequency, cumulative infiltration, and its contribution over matrix flow also increased.

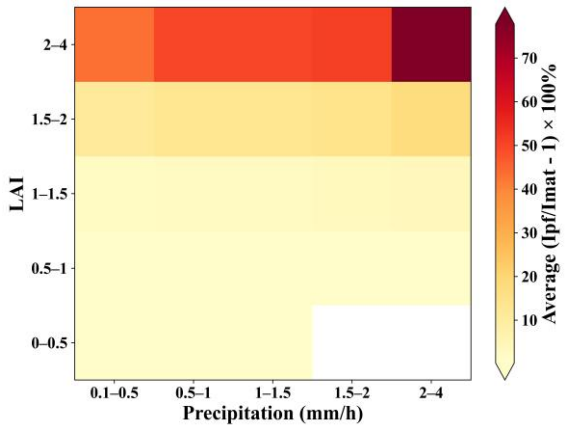

Figure 6. Heatmap Showing the Infiltration Increase Ratio Due to Soil Structure under Different Rainfall Intensities and LAI Levels

Moreover, the infiltration ratio was positively correlated with LAI, reflecting the effect of dense vegetation and complex root systems. However, low LAI values and torrential rain rarely co-occurred, especially as only the northwestern part of the plateau had poorly developed vegetation. Therefore, no data were recorded for areas with poorly developed vegetation under rainfall intensities of 1.5 – 4 mm/h.

4 CONCLUSIONS

In this study, we conducted a regional estimation of the K_0 of textural soils in the Loess Plateau based on soil texture data. Considering the influence of vegetation restoration on soil structure, we corrected the saturated hydraulic conductivity of structured soils using the LAI. By applying the Philip infiltration model and incorporating the Brooks-Corey soil water retention parameters, we systematically analyzed the impact of soil structural changes on hydraulic parameters and the regional water dynamics of the Loess Plateau.

Given the predominantly sandy soils in the Loess Plateau, the uncorrected saturated hydraulic conductivity was relatively high. After correcting for soil structural effects, regions with higher LAI showed a significant increase in K_s, while areas with lower LAI showed minimal change. The regional average saturated hydraulic conductivity increased from 61.95 mm/h to 80.47 mm/h, a relative increase of 29.8%, indicating that soil structures should not be neglected in the calculation of soil hydraulic properties.

The parameterized K_s in the Philip infiltration model led to increased infiltration under certain rainfall intensities. When soil structural effects were considered, the proportion of increased infiltration also showed variable patterns. Under different rainfall intensities and vegetation cover conditions, soil infiltration matched rainfall rate under lower rainfall intensities, where the contribution of preferential flow was minimal. In such cases, the regional increase in infiltration due to structural effects rose with increasing LAI and rainfall intensity. With the rapid progression of global climate change, the frequency and intensity of extreme rainfall events are expected to increase. Under future scenarios, vegetation conditions on the Loess Plateau are projected to improve significantly, which will enhance the development of soil macropores and render preferential flow an increasingly important contributor to soil water infiltration.

These findings highlight the significance of incorporating preferential flow−caused by plant root-induced macropores− into hydrological modeling and regional soil water infiltration analyses. This provides crucial insights for addressing practical challenges such as soil erosion and landslides on the Loess Plateau. This study also has certain limitations. For example, the shape parameters α and β in the parameterization were directly adopted from the original literature. Applying them to the Loess Plateau may introduce some bias. In the future, it is necessary to calibrate these parameters based on field measurements in the Loess Plateau to improve model adaptability.

5 ACKNOWLEDGEMENTS

This work was jointly supported by the Fundamental and Interdisciplinary Disciplines Breakthrough Plan of the Ministry of Education of China (JYB2025XDXM910), the National Natural Science Foundation of China (42571019, 42207002), the Natural Science Foundation of Gansu Province (24JRRA434), the Fundamental Research Funds for the Central Universities (lzujbky-2023-eyt01, lzujbky-2023-ey09), Natural Science Foundation of Gansu Province (24JRRA434), and the Fundamental Research Funds for the Central Universities (lzujbky-2023-eyt01 and lzujbky-2023-ey09). The data is provided by National Tibetan Plateau / Third Pole Environment Data Center (http://data.tpdc.ac.cn).

6 REFERENCES

Bonetti, S., Wei, Z. and Or, D., 2021. A framework for quantifying hydrologic effects of soil structure across scales. *Communications Earth & Environment*, 2(1), p.107.

Brooks, R.H., and A.J. Corey., 1964. *Hydraulic properties of porous media*. Colorado State Univ: Fort Collins, p.3.

Campbell, G. and Shiozawa, S., 1992. Prediction of hydraulic properties of soils using particle--size distribution and bulk density data. *International Workshop on Indirect Methods for Estimating the Hydraulic Properties of Unsaturated Soils*, pp.317–328.

Chen, H., Shao, M. and Li, Y., 2008. Soil desiccation in the Loess Plateau of China. *Geoderma*, 143(1–2), pp.91–100.

Chen, Y., Yang, K., He, J., Qin, J., Shi, J., Du, J. and He, Q., 2011. Improving land surface temperature modeling for dry land of China. *Journal of Geophysical Research*, 116(D20), D20104.

Clapp, R.B. and Hornberger, G.M., 1978. Empirical equations for some soil hydraulic properties. *Water Resources Research*, 14(4), pp.601–604.

Fan, L., Lehmann, P., Zheng, C. and Or, D., 2022. Vegetation-Promoted Soil Structure Inhibits Hydrologic Landslide Triggering and Alters Carbon Fluxes. *Geophysical Research Letters*, 49(18), p.e2022GL100389.

Fatichi, S., Or, D., Walko, R., Vereecken, H., Young, M.H., Ghezzehei, T.A., Hengl, T., Kollet, S., Agam, N. and Avissar, R., 2020. Soil structure is an important omission in Earth System Models. *Nature Communications*, 11(1), p.522.

Fu, B., Wang, S., Liu, Y., Liu, J., Liang, W. and Miao, C., 2017. Hydrogeomorphic Ecosystem Responses to Natural and Anthropogenic Changes in the Loess Plateau of China. *Annual Review of Earth and Planetary Sciences*, 45(1), pp.223–243.

Guan, N., Bi, H., Song, Y., Lu, S., Lin, D. and Han, J., 2024. Vegetation restoration is affecting the characteristics and patterns of infiltration in the Loess Plateau. *CATENA*, 243, p.108190.

Guo, L., Fan, B., Zhang, J. and Lin, H., 2018. Occurrence of subsurface lateral flow in the Shale Hills Catchment indicated by a soil water mass balance method. *European Journal of Soil Science*, 69(5), pp.771–786.

He, J., Yang, K., Tang, W., Lu, H., Qin, J., Chen, Y. and Li, X., 2020. The first high-resolution meteorological forcing dataset for land process studies over China. *Scientific Data*, 7(1), p.25.

Kang, W., Tian, J., Lai, Y., Xu, S., Gao, C., Hong, W., Zhou, Y., Pei, L. and He, C., 2022. Occurrence and controls of preferential flow in the upper stream of the Heihe River Basin, Northwest China. *Journal of Hydrology*, 607, p.127528.

Kang, W., Tian, J., Reemt Bogena, H., Lai, Y., Xue, D. and He, C., 2023. Soil moisture observations and machine learning reveal preferential flow mechanisms in the Qilian Mountains. *Geoderma*, 438, p.116626.

Kang, W., Zhang, Y., Zhao, W., Jia, A., Sun, C. and Tian, Z., 2021. Spatial Variation Characteristics of Soil Saturated Hydraulic Conductivity in a Desert-Oasis Ecotone. Journal of Soil and Water Conservation, 35(5), pp.137–143.

Lehmann, P., Von Ruette, J. and Or, D., 2019. Deforestation Effects on Rainfall-Induced Shallow Landslides: Remote Sensing and Physically-Based Modelling. *Water Resources Research*, 55(11), pp.9962–9976.

Li, Q., Shi, G., Shangguan, W., Nourani, V., Li, J., Li, L., Huang, F., Zhang, Y., Wang, C., Wang, D., Qiu, J., Lu, X. and Dai, Y., 2022. A 1 km daily soil moisture dataset over China using in situ measurement and machine learning. *Earth System Science Data*, 14(12), pp.5267–5286.

Ma, J., Zeng, R., Yao, Y., Meng, X., Meng, X., Zhang, Z., Wang, H. and Zhao, S., 2022. Characterization and quantitative evaluation of preferential infiltration in loess, based on a soil column field test. *CATENA*, 213, p.106164.

Myneni, R., Knyazikhin, Y. and Park, T., 2015. *MYD15A2H MODIS/Aqua Leaf Area Index/FPAR 8-Day L4 Global 500m SIN Grid V006*. Sioux Falls, South Dakota, USA: NASA Land Processes Distributed Active Archive Center.

Pan, H., Ran, Q., Hong, Y., Wang, J., Chen, X. and Ye, S., 2023. Long-term impacts of ecosystem restoration on saturated hydraulic conductivity in the Loess Plateau. *Journal of Hydrology*, 620, p.129337.

Parewa, H.P., Meena, V.S., Meena, S.K., Choudhary, A. and Kumar, M., 2023. Carbon management strategies for sustainable food production systems. *Agricultural Soil Sustainability and Carbon Management*, pp.69–98.

Ren, Z., Zhu, L., Wang, B. and Cheng, S., 2016. Soil hydraulic conductivity as affected by vegetation restoration age on the Loess Plateau, China. *Journal of Arid Land*, 8(4), pp.546–555.

Shangguan, W., Dai, Y., Liu, B., Zhu, A., Duan, Q., Wu, L., Ji, D., Ye, A., Yuan, H., Zhang, Q., Chen, D., Chen, M., Chu, J., Dou, Y., Guo, J., Li, H., Li, J., Liang, L., Liang, X., Liu, H., Liu, S., Miao, C. and Zhang, Y., 2013. A China data set of soil properties for land surface modeling. *Journal of Advances in Modeling Earth Systems*, 5(2), pp.212–224.

Singh, M., Sarkar, B., Sarkar, S., Churchman, J., Bolan, N., Mandal, S., Menon, M., Purakayastha, T.J. and Beerling, D.J., 2017. Stabilization of soil organic carbon as influenced by clay mineralogy. *Advances in Agronomy*, 148, pp.33–84.

Wang, N., Bi, H., Peng, R., Zhao, D. and Liu, Z., 2023a. Disparities in soil and water conservation functions among different forest types and implications for afforestation on the Loess Plateau. *Ecological Indicators*, 155, p.110935.

Wang, R., Dong, Z., Zhou, Z., Wang, N., Xue, Z. and Cao, L., 2020a. Effect of vegetation patchiness on the subsurface water distribution in abandoned farmland of the Loess Plateau, China. *Science of The Total Environment*, 746, p.141416.

Wang, R., Dong, Z., Zhou, Z., Wang, N., Xue, Z. and Cao, L., 2020b. Effect of vegetation patchiness on the subsurface water distribution in abandoned farmland of the Loess Plateau, China. *Science of The Total Environment*, 746, p.141416.

Wang, W., Li, S., Sun, J., Huang, Y., Han, F. and Li, Z., 2023b. Mechanism of groundwater recharge in the thick loess deposits by multiple environmental tracers. *Science of The Total Environment*, 897, p.165360.

Wen, X. and Deng, X., 2020. Current soil erosion assessment in the Loess Plateau of China: A mini-review. *Journal of Cleaner Production*, 276, p.123091.

Xiang, W., Si, B.C., Biswas, A. and Li, Z., 2019. Quantifying dual recharge mechanisms in deep unsaturated zone of Chinese Loess Plateau using stable isotopes. *Geoderma*, 337, pp.773–781.

Xue, D., Tian, J., Zhang, B., Kang, W., Zhou, Y. and He, C., 2024. Effects of vegetation types on soil wetting pattern and preferential flow in arid mountainous areas of northwest China. *Journal of Hydrology*, 642, p.131849.

Yang, F., Lu, H., Yang, K., He, J., Wang, W., Wright, J.S., Li, C., Han, M. and Li, Y., 2017. Evaluation of multiple forcing data sets for precipitation and shortwave radiation over major land areas of China. *Hydrology and Earth System Sciences*, 21(11), pp.5805–5821.

Yang, K., He, J., Tang, W., Qin, J. and Cheng, C.C.K., 2010. On downward shortwave and longwave radiations over high altitude regions: Observation and modeling in the Tibetan Plateau. *Agricultural and Forest Meteorology*, 150(1), pp.38–46.

Zhang B., Tian L., Zhao X. and Wu P., 2021. Feedbacks between vegetation restoration and local precipitation over the Loess Plateau in China. *Science China Earth Sciences*, 64(6), pp.920–931.

Zhang, Z., Si, B., Li, H. and Li, M., 2019. Quantify Piston and Preferential Water Flow in Deep Soil Using Cl− and Soil Water Profiles in Deforested Apple Orchards on the Loess Plateau, China. *Water*, 11(10), p.2183.

Zhao, Y. and Wang, L., 2021. Determination of groundwater recharge processes and evaluation of the 'two water worlds' hypothesis at a check dam on the Loess Plateau. *Journal of Hydrology*, 595, p.125989.

Zhu, P., Zhang, G., Wang, H. and Xing, S., 2020. Soil infiltration properties affected by typical plant communities on steep gully slopes on the Loess Plateau of China. *Journal of Hydrology*, 590, p.125535.

Zhu, P., Zhang, G. and Zhang, B., 2022. Soil saturated hydraulic conductivity of typical revegetated plants on steep gully slopes of Chinese Loess Plateau. *Geoderma*, 412, p.115717.